# Electroluminescence analysis of high efficiency $Cu(In, Ga)Se_2$ solar cells

Thomas Kirchartz, and Uwe Rau

# Electroluminescence analysis of high efficiency Cu(In,Ga)Se$_2$ solar cells

Thomas Kirchartz[a)] and Uwe Rau

*IEF5-Photovoltaik, Forschungszentrum Jülich, 52425 Jülich, Germany*

We compare the electroluminescence (EL) of polycrystalline ZnO/CdS/Cu(In,Ga)Se$_2$ heterojunction solar cells with similar band gaps but different open circuit voltages, indicating a difference in the electronic quality of the absorber. Temperature dependent EL measurements reveal that all cells feature transitions from donor-acceptor pair recombination at lower temperature to band to band recombination at higher temperatures. However, the less efficient cells show a longer transition range with donor-acceptor pair recombination still apparent at room temperature. We find further that the part of the room temperature spectrum that is due to band to band transitions in the respective cells is relatively broader than expected from a direct semiconductor with a homogeneous band gap. We analyze this spectral broadening by a model that accounts for band gap fluctuations of the absorber material. The experimental results show that the dominant part of this spectral broadening results from the intentional band gap grading and not from stochastic band gap fluctuations. We show further that the spectral EL emission is linked to the photovoltaic external quantum efficiency by electro-optical reciprocity. In a similar way, the external EL quantum efficiency is related to the open circuit voltage of the device. We verify experimentally that the difference between radiative and measured open circuit voltage determines the EL external quantum efficiency of the solar cell. The best Cu(In,Ga)Se$_2$ solar cell reaches an external light emitting diode quantum efficiency of around 0.1%. © *2007 American Institute of Physics.*
[DOI: 10.1063/1.2817959]

## I. INTRODUCTION

Solar cells made from the quaternary alloy Cu(In,Ga)Se$_2$ have achieved efficiencies $\eta > 19\%$,[1] i.e., more than any other thin film approach despite the polycrystallinity of the material. One commonly used characterization tool for photovoltaic absorber materials is the analysis of the photoluminescence, e.g., for the study of defect related properties. Photoluminescence measurements are mostly performed as a function of the position on the sample, i.e., spatially resolved,[2–5] or as a function of the energy of the emitted photons.[4,6–12] Photoluminescence allows deposited films as well as completed solar cells to be characterized in a contactless manner. Bauer *et al.*[6] showed further how to extract the maximum attainable open circuit voltage from absolute photoluminescence measurements.

The electroluminescence (EL) of CuInSe$_2$ has been subject to fundamental studies in 1970s,[9,13–15] where the material was considered for applications in optical communication. However, as a characterization method for Cu(In,Ga)Se$_2$ solar cells, EL has never been used, although electrical excitation followed by luminescence emission is the exact inverse of the photovoltaic process. This symmetry or reciprocity between the photovoltaic and the electroluminescent operation mode allows additional quantitative information to be extracted from EL as compared with photoluminescence.

In this paper we show, how EL measurements can serve as an efficient tool for the characterization of high efficiency Cu(In,Ga)Se$_2$ solar cells. First, we record the EL spectra in the temperature range $100\ \text{K} < T < 300\ \text{K}$ to investigate how the dominant radiative recombination path changes over temperature. To identify the character of the peaks in the spectrum, we perform injection level dependent measurements. In a second step, we show that the temperature dependence of the band to band peaks reveals information about the inhomogeneity of the band gap. These inhomogeneities are partly due to an intentional grading of the band gap versus depth, aiming at a better carrier collection, and partly due to lateral changes in the Ga content which strongly influence the local band gap. Mattheis *et al.*[16] have developed a theory describing the influence of a Gaussian distribution of band gaps on the emission spectrum. We show that with small refinements to this theory, the standard deviation $\sigma_g$ of the band gap inhomogeneities follows from the electroluminescence spectra. The extracted values are low, i.e., in the range of $15\ \text{meV} < \sigma_g < 27\ \text{meV}$. These values are comparable to those expected from band gap gradings,[16] which indicate that the lateral inhomogeneity might actually be rather low in these high efficiency devices. In a third step, we apply the reciprocity theorem between electroluminescent emission and quantum efficiency of a solar cell[17,18] to the room temperature measurements. We define an experimental, radiative open circuit voltage, considering the actual radiative recombination current—as measured with electroluminescence—and compare it to both the actual open circuit voltage and the ideal Shockley-Queisser (SQ) open circuit voltage.[19] The difference between the SQ limit and the radiative open circuit voltage is the loss due to a broadened band edge,[20] while the difference between the radiative and open circuit voltage ac-

---
[a)]Author to whom correspondence should be addressed. Electronic mail: t.kirchartz@fz-juelich.de.

TABLE I. Band gap energy $E_g$ (extrapolated from the quantum efficiency), Ga content from EDX measurements, and the Shockley-Queisser values under AM 1.5 G illumination for the saturation current density $J_0^{SQ}$, short circuit current density $J_{SC}^{SQ}$, and open circuit voltage $V_{OC}^{SQ}$. These values are compared to the measured values $J_{SC}$ and $V_{OC}$ and to the parameters $J_0^{rad}$ and $V_{OC}^{rad}$ for radiative recombination in the device as extracted from the combined electroluminescence and $Q_e$ analysis. The LED external quantum efficiencies $Q_{LED}$ refer to injected current densities of 200 mA cm$^{-2}$. The cell area of all samples is 0.5 cm$^2$.

|  | Sample A | Sample B | Sample C |
| --- | --- | --- | --- |
| $E_g$ (eV) | 1.21 | 1.19 | 1.24 |
| Ga content $x$ | 0.40 | 0.39 | 0.43 |
| $J_0^{SQ}$ (A cm$^{-2}$) at $E_g$ | $3.0 \times 10^{-18}$ | $6.2 \times 10^{-18}$ | $9.7 \times 10^{-19}$ |
| $J_{SC}^{SQ}$ (mA cm$^{-2}$) at $E_g$ | 38.8 | 39.8 | 37.3 |
| $V_{OC}^{SQ}$ (mV) at $E_g$ | 959 | 941 | 987 |
| $J_0^{rad}$ (A cm$^{-2}$) expt. | $3.5 \times 10^{-18}$ | $7.5 \times 10^{-18}$ | $2.3 \times 10^{-18}$ |
| $V_{OC}^{rad}$ (mV) expt. | 955 | 935 | 964 |
| $J_{SC}$ (mA cm$^{-2}$) measured | 31.2 | 31.6 | 29.0 |
| $V_{OC}$ (mV) measured | 739 | 719 | 700 |
| efficiency $\eta$ (%) | 18.2 | 17.4 | 16.1 |
| $Q_{LED}$ ($10^{-4}$) at 200 mA cm$^{-2}$ | 4.4 | 3.3 | 0.49 |

tually measured gives information on the light emitting diode (LED) quantum efficiency. We show how to connect the LED quantum efficiency to the open circuit voltage of the solar cell. It turns out that the Cu(In,Ga)Se$_2$ solar cells have LED quantum efficiencies approaching $Q_{LED} = 0.1\%$.

## II. EXPERIMENTS

The samples investigated were high efficiency Cu(In,Ga)Se$_2$ solar cells, fabricated by a three stage process[21] that enables efficiencies $\eta > 19\%$ (on a cell area of 0.5 cm$^2$)[22] to be achieved. After evaporation of the 1.5 $\mu$m thick Mo back contact on a glass substrate, the first stage of absorber deposition consists of the evaporation of In, Se, and Ga at a substrate temperature $T = 400\ ^\circ$C. The substrate temperature is then increased to $T \approx 610\ ^\circ$C and the second stage of Cu evaporation has begun. The evaporation of In and Ga is slightly decreased while the Se rate is kept constant throughout the whole process. In stage three, the substrate temperature remains constant, the Cu evaporation decreased, and the In and Ga evaporation is moved to a level slightly below stage one. After stage three, the Se deposition rate stays constant until the substrate has cooled down to 300 $^\circ$C. Reference 22 describes further details of the processing.

The three samples investigated in this article have a comparable band gap but strongly different open circuit voltages and efficiencies, which are reflected in different EL spectra. The values of the band gap $E_g$, as extrapolated from quantum efficiency measurements, the Ga content $x = (Ga)/(In+Ga)$ obtained from energy dispersive x-ray analysis (EDX), and cell parameters are given in Table I. Note that both, band gap energy $E_g$ and Ga content $x$ are not constant throughout the film thickness and over the sample area. Therefore the values given in Table I need to be interpreted with regard to the method used to determine them.[23] As described in Ref. 22 the Ga content is determined by EDX with penetration depths around 1 $\mu$m at cell thicknesses around 2.5 $\mu$m. Due to the strong grading of the band
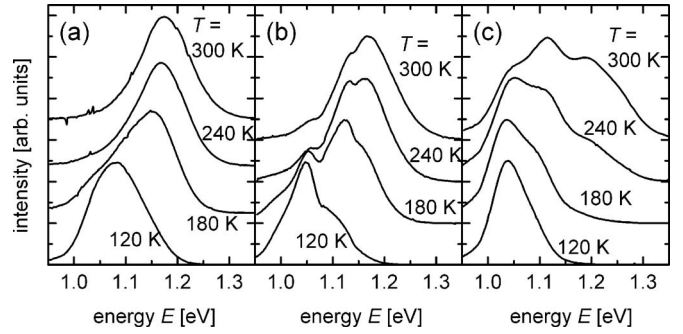


FIG. 1. Electroluminescence spectra from samples A to C at the temperatures $T = 120, 180, 240$, and 300 K. All samples show a clear transition from lower peak energies at low temperatures to higher energies at high temperatures. The intensity axis is proportional to the number of photons per time and energy interval.

gap versus cell depth, the minimum band gap at a point in the cell volume will be considerably smaller than that corresponding to the extracted Ga content. Hence the band gap energy in Table I yields a value similar to the spatially averaged minimum band gap where absorption starts while the Ga content is an average over the volume.

The electroluminescence is recorded with a liquid nitrogen cooled Ge detector attached to a monochromator with a 600 lines/mm grating blazed at $\lambda = 1000$ nm. The sample is mounted into an Oxford Cryodrive cryostat, while a Hewlett Packard pulse generator applies a rectangular shaped periodic voltage to the sample enabling the use of a lock-in amplifier.

## III. TEMPERATURE DEPENDENT MEASUREMENTS

### A. Results

Among the three solar cells investigated, sample A has the highest values for efficiency and open circuit voltage, followed by sample B, while sample C has the lowest performance as a solar cell. However, all three can be regarded as highly efficient polycrystalline thin film solar cells. The device quality is reflected in the temperature dependence of the electroluminescence spectra, which are recorded in the temperature range 100 K $< T <$ 300 K.

Firstly, we present the measured spectra and discuss their general features. Then, we look more closely at the position of the peaks as a function of temperature and identify the physical character of the peaks by excitation current dependent measurements. Finally, we discuss the differences between the samples.

For simplicity, Fig. 1 shows the electroluminescence at just four temperatures. All samples show a transition from lower peak energies at lower temperatures to higher peak energies at higher temperatures. The differences between the samples become apparent in the extent of the transition range and the number of visible peaks. In Fig. 1(a), we see that sample A shows one peak at $E_{\text{low }T} \approx 1.09$ eV for temperature $T = 120$ K and one peak around $E_{\text{high }T} \approx 1.17$ eV for higher temperatures $T = 240$ and 300 K. Only at $T = 180$ K, two contributions are distinguishable.

Figure 1(b) shows the spectra at the same temperatures for sample B. For temperatures $T = 120, 240$, and 300 K, the
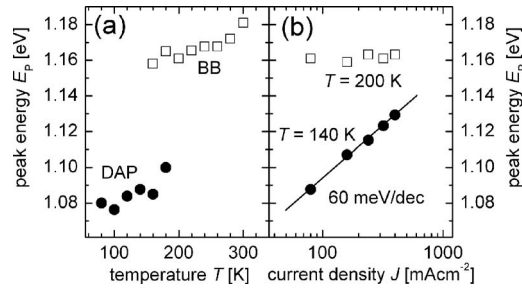
FIG. 2. (a) Dependence of the peak position in the Cu(In,Ga)Se$_2$ electroluminescence of sample A on temperature $T$ showing a transition between donor-acceptor pair (DAP) recombination at energies $E \approx 1.08$ eV and band to band (BB) recombination at $E \approx 1.16-1.17$ eV. (b) At $T=200$ K the peak position of the BB recombination does not depend on excitation current density, whereas at $T=140$ K we observe the characteristic blueshift (60 meV/decade) of a donor-acceptor pair transition.

spectra are again dominated by one peak, while at $T=180$ K, two very distinct peaks are visible. However, a closer look reveals that at the energy of the low temperature peak dominant at $T=120$ K, a smaller shoulder remains up to room temperature. For all temperatures shown, there are more than two peaks visible in the spectra.

Figure 1(c) shows that sample C has a variety of radiative transitions up to room temperature. The dominant low energy peak at $T=120$ K remains so up to $T=240$ K, and is still clearly visible at room temperature. Due to the three different peaks at room temperature, the spectrum is very broad.

For a detailed analysis, we fitted those spectra where more than one peak is clearly distinguishable and performed injection level dependent measurements, allowing to identify donor-acceptor pair transitions.[24] Figure 2(a) shows the evolution of peak position versus temperature for sample A. Below $T=120$ K, the only peak is around $E_{\text{low } T} \approx 1.09$ eV, between 160 and 180 K two peaks are distinguishable and are fitted by two Gaussians to determine the peak positions, while above 200 K only the high energy peak is left. The excitation level dependent measurements presented in Fig. 2(b) show a strong blueshift of 60 meV/decade below the transition range, at $T=140$ K. Above the transition no peak shift with increasing temperature is visible. This leads to the conclusion that the low energy transition, dominating at low temperatures, is a donor-acceptor pair (DAP) transition, while the high energy peak is the band to band (BB) transition.

Figure 3 shows the equivalent measurements for the case of sample B. The spectra were fitted with Lorentian peak shapes instead of Gaussians to achieve a better fit. The excitation dependent measurements shown in Fig. 3(b) were performed at $T=100$, 200, and 300 K, and reveal that the low energy peak around $E=1.05$ eV features a blueshift with increasing injection current only for the lowest temperature. This blueshift is considerably smaller than that of sample A. Since only one peak shows a clear shift at low temperatures, unambiguous identification of the other peaks becomes impossible with the methods used here. The most probable interpretation is that the high energy peak is the band to band peak [marked with BB in Fig. 3(a)], the second peak is a free
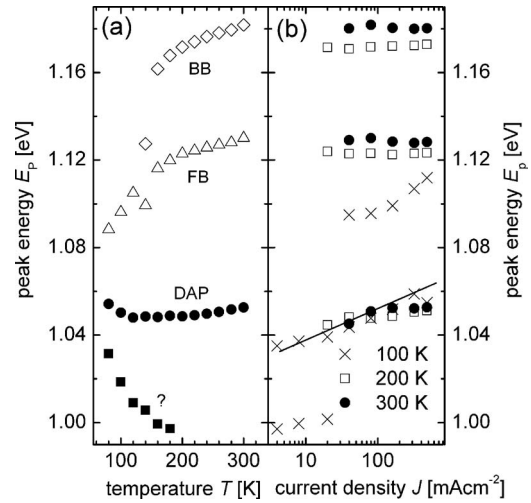


FIG. 3. (a) Dependence of the peak position in the electroluminescence of sample B on temperature $T$ showing up to four peaks at the different temperatures. In contrast to sample A, sample B has a contribution from sub-band-gap transitions up to room temperature. (b) Excitation current dependent measurements only identify the peak around $E \approx 1.05$ eV as a DAP transition at the lowest temperature investigated ($T=100$ K). For all other temperatures and energies, there is no clear blueshift visible.

to bound peak [marked with FB in Fig. 3(a)], and the third is the donor-acceptor pair peak (marked with DAP). The origin of the lowest energy peak, visible only at low temperatures, is not yet understood.

Figure 4(a) shows that sample C features only three peaks, which we could fit well with Gaussians. The excitation level dependent measurements in Fig. 4(b) show a small blueshift for the low energy peak at $T=140$ K and $T=200$ K. Thus, the interpretation of the peaks as band to band, free to bound, and donor-acceptor pair follows the above mentioned suggestion for sample B.
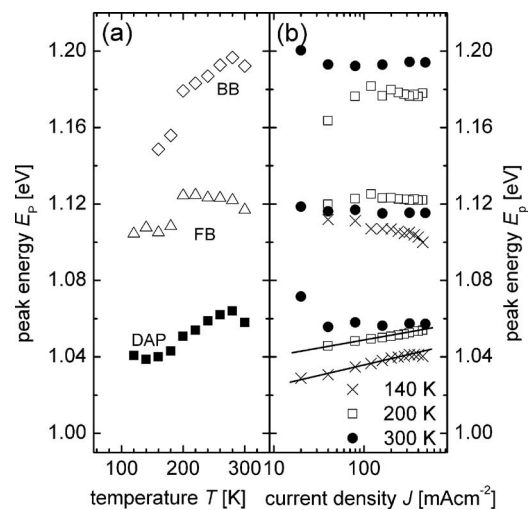


FIG. 4. (a) Dependence of the peak position in the electroluminescence of sample C on temperature $T$ showing three peaks, which are identified as donor-acceptor pair (DAP), free to bound (FB), and band to band (BB) in order of increasing energy. The spectrum of sample C shows a contribution of several sub-band-gap transitions up to room temperature. (b) Similar as for sample B, the excitation current dependent measurements only identify the lowest energy peak at $T=140$ and 200 K as a DAP transition, while all other transitions do not show a blueshift.

Comparing all three samples leads to three conclusions: (i) The less efficient cells show more peaks and especially broader spectra at room temperature. We extracted the full width at half maximum (FWHM) of the room temperature spectra, which amounts to FWHM=107, 123, and 231 meV for samples A–C, respectively. Hence, sample C especially has a strongly broadened room temperature spectrum with several peaks leading to a FWHM being more than two times that of sample A. (ii) All spectra are considerably broader than one would expect from a direct semiconductor. We propose that for low temperatures this broadening is a result of a DAP transition, broadened due to *potential fluctuations*,[25–28] whereas at higher temperatures the broadening of a BB transition is due to lateral *band gap fluctuations*[16,20–29] and the intentional band gap grading. (iii) The blueshift with increasing injection current is visible for all samples in the low energy peak at low temperatures. However, the DAP peaks of both samples B and C have much smaller blueshifts than for sample A (15 meV/decade for sample B and 12 meV/decade for sample C). Explaining the exact strength of the blueshift is an issue still to be resolved.

## B. Interpretation in terms of compositional inhomogeneities

The temperature dependent measurements show that all samples have a very broad luminescence at room temperature because of band gap fluctuations. Furthermore, samples B and C have additionally broadened luminescence, since a contribution of sub-band-gap recombination remains up to room temperature.

The Ga content of these $Cu(In,Ga)Se_2$ solar cells is changed intentionally over depth to achieve a better charge collection. In addition lateral changes in composition may occur, together leading to a dependence of the band gap on all three spatial coordinates. Since the band gap determines the peak positions of the band to band transitions, the degree of inhomogeneity may be measured by electroluminescence. As introduced in Refs. 16 and 20, we assume a Gaussian distribution of band gaps centered around an average band gap $\bar{E}_g$ with a standard deviation $\sigma_g$. The first order approach of a step-function-like local absorptance $a_{loc}(E)=0$ for energies $E < E_g$ and $a_{loc}(E)=1$ for $E > E_g$, as assumed in Refs. 16 and 20, leads to an error-function-like global absorptance,

$$a_{glob}(E, \bar{E}_g) = \int_0^\infty a_{loc}(E_g) \exp\left[-\left(\frac{E_g - \bar{E}_g}{\sqrt{2}\sigma_g}\right)^2\right] \frac{dE_g}{\sqrt{2\pi}\sigma_g}$$
$$= \frac{1}{2}\,\mathrm{erfc}\left(\frac{\bar{E}_g - E}{\sqrt{2}\sigma_g}\right). \quad (1)$$

The emission spectrum follows from Kirchhoff's law, i.e., the multiplication of the global absorptance with the blackbody spectrum at the temperature of the sample. This simple approach already reveals that the standard deviation $\sigma_g$ is contained twofold in the dependence of the peak energies of the band to band transition on temperature. First, the distance between the band gap and electroluminescence peak becomes larger with larger standard deviation $\sigma_g$, and the slope of the peak positions versus temperature becomes

steeper with higher $\sigma_g$. However, in order to get a reasonable fit for the spectra, it was necessary to refine the model. For the absorption, we used a square-root-like absorption coefficient $\alpha$ above the band gap $E_g$ and an Urbach tail below the band gap. The Urbach tail was allowed to have a linearly temperature dependent Urbach energy $E_U$. The two parts of the absorption coefficient were chosen in a way that they are continuously differentiable. Considering these boundary conditions the absorption coefficient follows as

$$\alpha = \begin{cases} \alpha_0 \sqrt{\dfrac{E - E_g}{kT}} & \text{for } E > E_g + E_U/2 \\ \alpha_0 \exp(E - E_g/E_U)\sqrt{\dfrac{E_U}{2\exp(1)kT}} & \text{for } E < E_g + E_U/2, \end{cases}$$
$$(2)$$

where $k$ is the Boltzmann constant. The local absorptance $a_{loc}$ is approximated as $a_{loc}(E)=[1-\exp(-\alpha d_{eff})]$, where $d_{eff}$ is an effective optical thickness, which accounts for the beneficial effect of light trapping on the optical path of insufficiently absorbed light. The global absorptance $a_{glob}$ is then

$$a_{glob}(E, \bar{E}_g) = \int_0^\infty a_{loc}(E_g) \exp\left[-\left(\frac{E_g - \bar{E}_g}{\sqrt{2}\sigma_g}\right)^2\right] \frac{dE_g}{\sqrt{2\pi}\sigma_g}.$$
$$(3)$$

As outlined in Sec. IV the quantum efficiency, and not the absorptance, is responsible for the shape of the electroluminescence spectrum. However, in the present case, using the absorptance given in Eq. (3), and then applying Kirchhoff's law, is a good approximation. Given the fact that the band to band peaks, as shown in Figs. 2(a), 3(a), and 4(a), are all well below the band gap as presented in Table I, the peak shape and position of electroluminescence spectra are mostly determined by optical effects and not by an energy dependent collection efficiency. This is due to the fact that for small absorption coefficients the generation rate becomes small as well as independent of depth. The collection efficiency, being a function of depth, is now independent of energy and simply a constant factor which does not change the shape of the spectrum.

## C. Discussion

Figure 5 shows the EL spectra of sample A for temperatures of $T=200$ K (circles), 240 K (triangles), and 300 K (squares) together with the fits following Eq. (3). The band gap was fixed at $E_g=1.21$ eV and the fit parameters were the standard deviation $\sigma_g$, the linearly dependent Urbach tail $E_U(T)$, and the prefactor of the absorption coefficient times the effective thickness $\alpha_0 d_{eff}$. We fitted the spectra at $T=200$ and 300 K directly and added the spectrum at $T=240$ K to show that the shape of this spectrum is still well approximated. The resulting values are $\sigma_g=26.6$ meV, $E_U(T)=(0.034T+7.4)$ meV, and $\alpha_0 d_{eff}=1.043$.

As shown in Figs. 1(b) and 1(c) the room temperature spectra of samples B and C do not consist solely of the single band to band peak. A fit of the whole spectrum to obtain the standard deviation of the band gap distribution is therefore
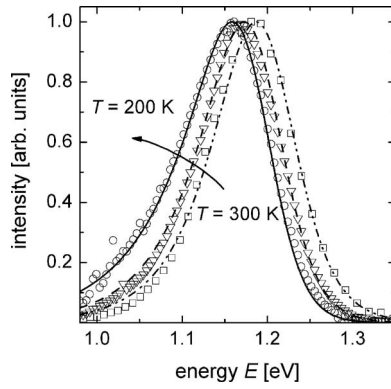
FIG. 5. The electroluminescence spectra of sample A at temperatures $T$ =200 K (circles), 240 K (triangles), and 300 K (squares). The experimental spectra are fitted with an absorptance following Eq. (3) multiplied by a blackbody spectrum [see Eq. (5)].

not possible. Instead, we use the temperature dependence of the band to band peaks shown in Figs. 2(a), 3(a), and 4(a). In order to fit the peak positions to extract the standard deviation, we adopted a simpler approach for the absorption coefficient neglecting Urbach tails. The results are shown in Fig. 6 together with the band to band transitions of samples A–C. The standard deviations resulting from the fit of the peak positions and the fit of the whole spectra are nearly the same (comparing $\sigma_g$=26.4 meV from fitting the peak positions to $\sigma_g$=26.6 meV from the fit of the spectra shown in Fig. 5). Hence, we conclude that (i) the standard deviation $\sigma_g$ is a rather robust parameter and (ii) that the method of determining $\sigma_g$ must somehow consider the fact that the band to band peaks are several tens of meV below the band gap. From the two results of a high standard deviation of the band gap distribution, the distance between the band gap and peak positions as well as the temperature dependence of the peaks, only the temperature dependence of the peaks is suitable for the determination of the standard deviation.

The sub-band-gap absorption, however, has to be considered by a suitably modeled absorption coefficient. Although only a slightly more sophisticated model with Urbach tails is capable of describing the peak shapes, the very simple model already yields a similar result, when only considering the peak positions. Due to the presence of more than one peak in the room temperature spectra for samples B and C, only the
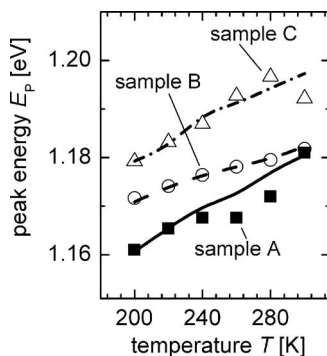


FIG. 6. Peak positions of the band to band transitions of samples A–C as a function of temperature. The standard deviations derived from fitting the peak positions (lines) are $\sigma_g$=26.4 meV (sample A), $\sigma_g$=16.6 meV (sample B), and $\sigma_g$=25.0 meV (sample C).

simpler model is applicable. From this model, the resulting standard deviations of samples B and C are $\sigma_g$=16.5 meV and $\sigma_g$=25.0 meV, respectively.

The low standard deviations of peaks in the spectra of the three cells are of the order of the standard deviations associated with a band gap grading, as calculated in Ref. 16. The lateral inhomogeneity of the samples might therefore be very small, and the fact that the most efficient cell (sample A) has the highest standard deviation may be a consequence of a large, intentional grading used to increase carrier collection.

## IV. RECIPROCITY BETWEEN ELECTROLUMINESCENCE AND PHOTOVOLTAIC QUANTUM EFFICIENCY

### A. Theory

Electroluminescence and photovoltaic energy conversion of a solar cell (likewise of a light emitting diode) are complementary physical actions. This reciprocity is expressed quantitatively by the relation[17]

$$\phi_{em}(E) = Q_e(E)\phi_{bb}(E)\left[\exp\left(\frac{qV}{kT}\right) - 1\right], \qquad (4)$$

which connects the emitted excess spectral photon density $\phi_{em}(E)$ with the photovoltaic external quantum efficiency $Q_e(E)$. In Eq. (4), $V$ is the internal voltage at the $p$-$n$ junction, $kT/q$ is the thermal voltage, and

$$\phi_{bb}(E) = \frac{2\pi E^2/(h^3c^2)}{\exp(E/kT) - 1} \approx \frac{2\pi E^2}{h^3c^2}\exp\left(\frac{-E}{kT}\right) \qquad (5)$$

is the spectral photon density of a blackbody.

As outlined in Ref. 17 the reciprocity relation [Eq. (4)] relies on the validity of another reciprocity theorem, derived by Donolato.[30] The Donolato theorem connects the carrier concentration in the dark under applied bias with the collection efficiency of photogenerated charge carriers under illumination. As shown in Refs. 31–34, Donolato's theorem is valid for a very generalized diffusive transport[35] of minority carriers with spatially fluctuating band gaps, lifetimes, mobilities, and equilibrium minority carrier concentrations. Thus, the Donolato theorem as well as Eq. (4) also holds for Cu(In,Ga)Se$_2$ solar cells, where the Ga content and hence the band gap change as a function of depth.

Equation (4) is an important tool for the analysis of optoelectronic devices as it connects two quantities—$\phi_{em}(E)$ and $Q_e(E)$—that are accessible via two independent experiments. Furthermore, we may use Eq. (4) to derive the saturation current density $J_0^{rad}$ for radiative recombination of the device under consideration as[18]

$$J_0^{rad} = q\int_0^\infty Q_e(E)\phi_{bb}(E)dE, \qquad (6)$$

where $q$ is the elementary charge. The short circuit current density $J_{SC}$ is calculated by a similar equation

$$J_{SC} = q \int_0^\infty Q_e(E) \phi_{sun}(E) dE, \tag{7}$$

where $\phi_{sun}(E)$ is the solar spectrum. As outlined in Ref. 18 we can therefore calculate the radiative open circuit voltage,

$$V_{OC}^{rad} = \frac{kT}{q} \ln\left(\frac{J_{SC}}{J_0^{rad}} + 1\right), \tag{8}$$

for any given real device from its photovoltaic external quantum efficiency. Note that $V_{OC}^{rad}$ as given in Eq. (8) is now related to the EL emission of the device and, therefore, differs from $V_{OC}^{SQ}$ which assumes an abrupt absorption edge of the photovoltaic absorber material at its band edge energy.[19]

The external quantum efficiency $Q_{LED}(V)$ of the device if operated as a LED is a single number defined by

$$Q_{LED}(V) = \frac{J_{rad}(V)}{J_{nr}(V) + J_{rad}(V)} = \frac{J_0^{rad} \exp(qV/kT)}{J_{nr}(V) + J_{rad}(V)}. \tag{9}$$

Since the radiative recombination current density $J_{rad}$ in Eq. (9) may depend in a different way on the applied voltage than the nonradiative recombination current density $J_{nr}$, the LED quantum efficiency $Q_{LED}(V)$ may change with voltage. If the device is operated under open circuit, we have

$$J_{nr} + J_{rad} = J_{SC}. \tag{10}$$

This is because at $V = V_{OC}$ the overall current has to be zero. Combining Eqs. (8)–(10) finally yields[17,18]

$$\Delta V_{OC} = V_{OC}^{rad} - V_{OC} = -\frac{kT}{q} \ln[Q_{LED}(V_{OC})]. \tag{11}$$

Equation (11) represents a second reciprocity relation that connects the real open circuit voltage $V_{OC}$ of the device with the external LED quantum efficiency. As pointed out by Markvart the voltage loss defined in Eq. (11) is an entropy term accounting for irreversible losses due to nonradiative recombination.[36] Thus, the LED quantum efficiency measures the entropy generation in a solar cell due to nonradiative recombination.

## B. Discussion

From the band gaps as listed in Table I the cell parameters ($J_0^{SQ}$, $J_{SC}^{SQ}$, and $V_{OC}^{SQ}$) of a Shockley-Queisser cell are calculated and presented in Table I. The cell in the Shockley-Queisser limit is a cell with step-function-like absorptance and exclusively radiative recombination. The saturation current of real solar cells is different in two respects: (i) The absorptance is not step-function-like, and (ii) nonradiative recombination exists. Both effects are responsible for the difference $\Delta V_{OC}^{tot} = V_{OC}^{SQ} - V_{OC}$ between Shockley-Queisser limit $V_{OC}^{SQ}$ and actual open circuit voltage. To distinguish between those two effects, we introduce the experimental radiative open circuit voltage $V_{OC}^{rad}$. The experimental radiative open circuit voltage answers the question of how large $V_{OC}$ would be if there was only radiative recombination, but the quantum efficiency was the same as for the actual device (i.e., no step function). To determine $V_{OC}^{rad}$, we need to calculate the radiative saturation current density $J_0^{rad}$ from Eq. (6), which is the integral over the properly scaled electroluminescence
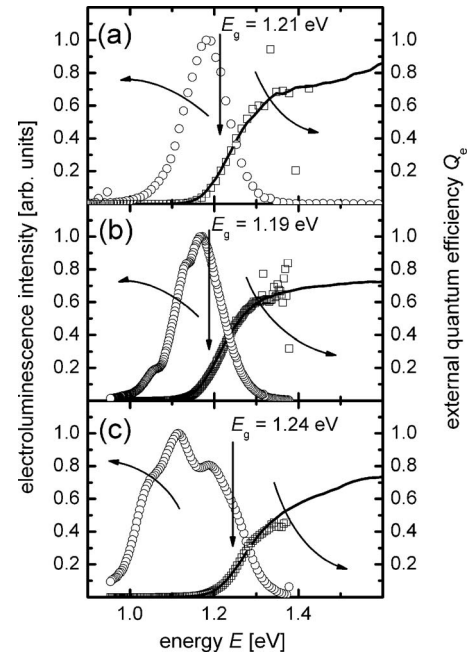


FIG. 7. The electroluminescence spectra at $T = 300$ K (open circles) yield a recalculated external quantum efficiency $Q_{e,EL}$ (open squares), which is in good agreement with the measured photovoltaic external quantum efficiency $Q_{e,dir}$ (lines). The scaling of the electroluminescence with the quantum efficiency enables the calculation of the radiative saturation current densities $J_0^{rad}$ and the radiative open circuit voltages $V_{OC}^{rad}$ for the three cells.

spectrum. The scaling is accomplished by using the reciprocity theorem of Eq. (4). The quantum efficiency calculated from the electroluminescence spectrum is compared with the directly measured quantum efficiency as shown in Fig. 7 for the samples A–C. Since the directly measured solar cell quantum efficiency is calibrated (lines) we can adjust the quantum efficiency from electroluminescence (squares) and subsequently determine $J_0^{rad}$. Note that although we can calculate the product $Q_e(E)\phi_{bb}(E)$ in absolute units, we cannot measure $\phi_{em}(E) = Q_e(E)\phi_{bb}(E)[\exp(qV/kT) - 1]$ with this approach, since the internal voltage $V$ is not directly accessible.

Since we know the short circuit currents from current/voltage measurements under AM 1.5 G illumination, we are now able to compute the experimental, radiative open circuit voltages. Table I presents the resulting values. This allows us to define two open circuit voltage differences, namely, $\Delta V_{OC}^* = V_{OC}^{SQ} - V_{OC}^{rad}$ and $\Delta V_{OC} = V_{OC}^{rad} - V_{OC}$, the latter being identical to the definition of Eq. (11). The broadened luminescence leads to a broadened absorption edge and subsequently causes the experimental radiative saturation current density to be higher than without the broadening. This loss is measured with $\Delta V_{OC}^* = V_{OC}^{SQ} - V_{OC}^{rad}$. For samples A and B, which feature only one dominant peak, this loss is only $\Delta V_{OC}^* = 4$ mV (sample A) and $\Delta V_{OC}^* = 6$ mV (sample B). But for the strongly broadened luminescence of sample C, the loss is $\Delta V_{OC}^* = 23$ mV. As long as the spectrum is dominated by the band to band transition, the determination of the standard deviation of inhomogeneous band gaps, as carried out in section B, is in principle also possible only using $\Delta V_{OC}^*$. Reference 20 gives a simple equation for the voltage loss $\Delta V_{OC}^{inhom} = \sigma_g^2/2kTq$ caused by an inhomogeneous band gap with standard deviation $\sigma_g$ as compared to a sample with a
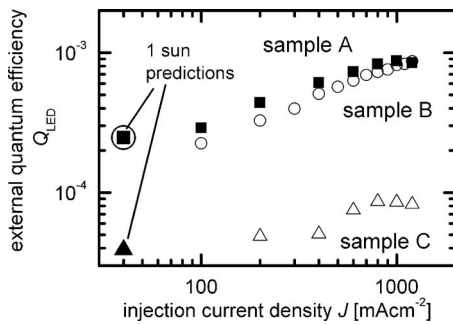
FIG. 8. External LED quantum efficiency as a function of injection current for samples A–C. The experimental values begin at current densities corresponding to two or more suns due to the limited sensitivity of the setup for absolute measurements. Nevertheless, the one sun predictions, derived from the open circuit voltage and the room temperature electroluminescence spectrum, correspond very well to the experimental data.

homogeneous band gap. We assume that the broadening of the room temperature spectrum is due to the inhomogeneity of the band gap—and hence broadening of the band to band transition—and *in addition* due to transitions via levels in the band gap. Under this assumption, the open circuit voltage difference $\Delta V_{OC}^*$ will be an upper limit for the voltage loss $\Delta V_{OC}^{inhom}$. Hence we find upper limits for the standard deviation, namely, $\sigma_g = 14.4$ meV for sample A, 17.7 meV for sample B, and 34.6 meV for sample C. Samples B and C behave as expected, since the value is larger than that from the temperature dependence. The difference is very small for sample B ($17.7 - 16.5$ meV) while it is significantly larger for sample C ($34.6 - 25.0$ meV). This is in accordance with the fact that the broadening due to additional sub-band-gap peaks is small for sample B and very pronounced for sample C. For sample A, however, the true standard deviation of the inhomogeneities as obtained from the fits in Fig. 5 is $\sigma_g = 26.6$ meV, which is larger than the value extracted from $\Delta V_{OC}^*$ as explained above. This reminds us of the fact that the band gap determination via an extrapolation of $\alpha^2$ versus energy $E$ is not accurate enough to determine the band gap with meV resolution. Therefore, we conclude that the method of determining the standard deviation $\sigma_g$ of the band gap inhomogeneities via the voltage difference $\Delta V_{OC}^* = V_{OC}^{SQ} - V_{OC}^{rad}$ is in principle possible but much more error prone than the determination via the temperature dependence. However, the value of $\Delta V_{OC}^*$ is even more general than the value of the standard deviation $\sigma_g$, since it also takes into account other sources of emission broadening that cause the radiative open circuit voltage to decrease.

Obviously, the largest part of the total loss in open circuit voltage is caused by nonradiative recombination, namely, $\Delta V_{OC} = 216$ mV for samples A and B and $\Delta_V^{OC} = 264$ mV for sample C. This loss solely determines the efficiency of the device as LED. According to Eq. (11) we can calculate the external LED quantum efficiency $Q_{LED}$ at an injection current $J_{inj} = J_{SC}$ from the voltage loss $\Delta V_{OC}$. Figure 8 compares these predictions with measured values of the external LED quantum efficiency. For absolute optical power measurements we used a calibrated low power optical sensor from Coherent, equipped with a Ge detector. To calculate the optical power from the number of detected photons, the

spectrum is assumed to be monochromatic. The Ge detector has insufficient sensitivity to measure the optical power from the solar cells for injection currents as low as $J = 30$ mA cm$^{-2}$ corresponding to one sun conditions (i.e., corresponding to the measured $J_{SC}$). Therefore the prediction cannot be directly checked. However, the predicted values fit very well to the measured data. Considering the uncertainties when measuring absolute optical power, the agreement is excellent.

It is clear from the measurements of all three samples shown in Fig. 8 that the maximum LED efficiency is far above one sun conditions. The maximum room temperature LED quantum efficiency approaches $Q_{LED} = 0.1\%$ at injection current densities around $J = 1$ A cm$^{-2}$.

## V. SUMMARY

We have compared the electroluminescence of three polycrystalline ZnO/CdS/Cu(In,Ga)Se$_2$ heterojunction solar cells with similar band gaps but different open circuit voltages and consequent efficiencies, indicating a difference in the electronic quality of the absorber. Temperature dependent electroluminescence measurements have revealed that all cells feature transitions from donor-acceptor pair recombination at lower temperature to band to band recombination at higher temperatures. However, the less efficient cells show a longer transition range with donor-acceptor pair recombination still apparent at room temperature, while the best cell has a very shallow transition range $160$ K $< T < 180$ K. The degree of compositional fluctuation causing the inhomogeneity of the band gap is extracted from the temperature dependence of the band to band peaks. The resulting values for the standard deviation are between 16.5 and 26.6 meV. These values are comparable to those predicted for strong band gap gradings, indicating that the influence of lateral inhomogeneities may indeed be small. We use reciprocity relations between electroluminescent and photovoltaic action of solar cells to identify the losses in open circuit voltage due to broadened luminescence and to nonradiative recombination. Finally we are able to predict the external LED quantum efficieny and verify our calculations experimentally. The measurements show that Cu(In,Ga)Se$_2$ solar cells reach external LED efficiencies of around 0.1%.

## ACKNOWLEDGMENTS

[1] M. A. Contreras, B. Egaas, K. Ramanathan, J. Hiltner, A. Swartzlander, F. Hasoon, and R. Noufi, Prog. Photovoltaics **7**, 311 (1999).
[2] M. J. Romero, C.-S. Jiang, R. Noufi, and M. M. Al-Jassim, Appl. Phys. Lett. **86**, 143115 (2005).
[3] M. J. Romero, C.-S. Jiang, J. Abushama, H. R. Moutinho, M. M. Al-Jassim, and R. Noufi, Appl. Phys. Lett. **89**, 143120 (2006).
[4] L. Gütay and G. H. Bauer, Thin Solid Films **515**, 6212 (2007).
[5] K. Bothe, G. H. Bauer, and T. Unold, Thin Solid Films **403**, 453 (2002).
[6] G. H. Bauer, R. Brüggemann, S. Tardon, S. Vignoli, and R. Kniese, Thin

Solid Films **480**, 410 (2005).

[7] G. Dagan, F. Abou-Elfotouh, D. J. Dunlavy, R. J. Matson, and D. Cahen, Chem. Mater. **2**, 287 (1990).

[8] G. Massé and E. Redjai, J. Appl. Phys. **56**, 1154 (1984).

[9] P. Migliorato, J. L. Shay, H. M. Kasper, and S. Wagner, J. Appl. Phys. **46**, 1777 (1975).

[10] S. Shimakawa, K. Kitani, S. Hayashi, T. Satoh, Y. Hashimoto, Y. Takahashi, and T. Negami, Phys. Status Solidi A **203**, 2630 (2006).

[11] S. Zott, K. Leo, M. Ruckh, and H. W. Schock, Appl. Phys. Lett. **68**, 1144 (1996).

[12] S. Zott, K. Leo, M. Ruckh, and H. W. Schock, J. Appl. Phys. **82**, 356 (1997).

[13] P. W. Yu, Y. S. Park, S. P. Faile, and J. E. Ehret, Appl. Phys. Lett. **26**, 717 (1975).

[14] P. Migliorato, B. Tell, J. L. Shay, and H. M. Kasper, Appl. Phys. Lett. **24**, 227 (1974).

[15] P. M. Bridenbaugh and P. Migliorato, Appl. Phys. Lett. **26**, 459 (1975).

[16] J. Mattheis, U. Rau, and J. H. Werner, J. Appl. Phys. **101**, 113519 (2007).

[17] U. Rau, Phys. Rev. B **76**, 085303 (2007).

[18] T. Kirchartz, U. Rau, M. Kurth, J. Mattheis, and J. H. Werner, Thin Solid Films **515**, 6238 (2007).

[19] W. Shockley and H. J. Queisser, J. Appl. Phys. **32**, 510 (1961).

[20] U. Rau and J. H. Werner, Appl. Phys. Lett. **84**, 3735 (2004).

[21] A. M. Gabor, J. R. Tuttle, D. S. Albin, M. A. Contreras, R. Noufi, and A. M. Hermann, Appl. Phys. Lett. **65**, 198 (1994).

[22] P. Jackson, R. Würz, U. Rau, J. Mattheis, M. Kurth, T. Schlötzer, G. Bilger, and J. H. Werner, Prog. Photovoltaics **15**, 507 (2007).

[23] T. Dullweber, U. Rau, M. A. Contreras, R. Noufi, and H.-W. Schock, IEEE Trans. Electron Devices **47**, 2249 (2000).

[24] E. Zacks and A. Halperin, Phys. Rev. B **6**, 3072 (1972).

[25] B. J. Shklovskii and A. L. Efros, *Electronic Properties of Doped Semiconductors* (Springer, Berlin, 1984).

[26] I. Dirnstorfer, Mt. Wagner, D. M. Hoffmann, M. D. Lampert, F. Karg, and B. K. Meyer, Phys. Status Solidi A **168**, 163 (1998).

[27] A. Bauknecht, S. Siebentritt, J. Albert, and M. Ch. Lux-Steiner, J. Appl. Phys. **89**, 4391 (2001).

[28] S. Siebentritt, N. Papathanasiou, and M. Ch. Lux-Steiner, Physica B **376–377**, 831 (2006).

[29] J. H. Werner, J. Mattheis, and U. Rau, Thin Solid Films **480-481**, 399 (2005).

[30] C. Donolato, Appl. Phys. Lett. **46**, 270 (1985).

[31] M. A. Green, J. Appl. Phys. **81**, 269 (1997).

[32] K. Misiakos and F. A. Lindholm, J. Appl. Phys. **58**, 4743 (1985).

[33] T. Markvart, IEEE Trans. Electron Devices **ED-43**, 1034 (1996).

[34] U. Rau and R. Brendel, J. Appl. Phys. **84**, 6412 (1998).

[35] J. A. del Alamo and R. M. Swanson, IEEE Trans. Electron Devices **ED-31**, 1878 (1984).

[36] T. Markvart, Appl. Phys. Lett. **91**, 064102 (2007).